Supplementary Information

Endosomal GPCR signaling turned off by negative feedback actions of PKA and v-ATPase

Alexandre Gidon[1], Mohammad M. Al-Bataineh[2], Frederic G. Jean-Alphonse[1], Hilary Stevenson[3], Tomoyuki Watanabe[4], Claire Louet[1], Ashok Khatri[4], Guillermo Calero[3], Núria M. Pastor-Soler[2], Thomas J. Gardella[4], and Jean-Pierre Vilardaga[1,*]

[1]*Laboratory for GPCR Biology, Department of Pharmacology & Chemical Biology, and* [2]*Renal-Electrolyte Division, and* [3]*Department of Structural Biology Department of Medicine, University of Pittsburgh, School of Medicine, Pittsburgh, PA 15261, USA*; [4]*Endocrine Unit, Massachusetts General Hospital and Harvard Medical School, Boston, MA 0114, USA.*

[*]To whom correspondence should be addressed. E-mail: jpv@pitt.edu

Supplementary Note

Peptide synthesis. Peptide analogs were synthesized on an automated Peptide Synthesizer (model 431A; Applied Biosystems, Foster City, CA) with Fmoc solid-phase chemistry using the classical N,N-Dicyclohexyl Carbodiimide (DCC)/1 – Hydroxybenzotriazole (HOBt) activation. The N-terminal amino acid was protected with a t-boc group for the peptides requiring a site-specific fluorescent label. An ivDde side-chain protection group was used for Lys13 for labeling purposes. The selective deprotection of the ivDde functional group was achieved with several treatments (5 min each) of the peptide resins with 2% hydrazine monohydrate in DMF. A positive ninhydrin test confirmed removal of the protection group.

Fluorescent dye labeling and cleavage of peptides. Peptide resins were coupled with 4-fold molar excess of 5-Carboxy-tetramethylrhodmine (5-TMR) or 5- carboxy-fluorescein (5-FAM) using Diisopropyl-Carbodiimide (DIC)/HOBt activation. The mixture was left to react overnight. Resins were washed six times with DMF and twice with methanol to remove the unreacted dye and the activators. Dried resins were cleaved with a cleavage cocktail K, containing TFA/thioanisole/water/phenol/ethanedithiol (82.5:5:5:5:2.5 v/v) for 3 h at room temperature. Crude peptides were precipitated and washed twice in cold methyl tert-butyl ether (MTBE). Precipitates were then dissolved in 20% CH_3CN/0.1% TFA.dH_2O and freeze-dried.

Peptide purification. Crude peptides were dissolved in 20% CH_3CN/0.1% TFA.dH_2O and purified on a 250 × 20 mm reversed-phase column (Higgins Analytical Targa C18 Semi-Preparative) and a Waters HPLC using a 20–40% B gradient in 20 min at a flow rate of 15 ml/min. Buffer A was 0.1% TFA in dH_2O and Buffer B was 0.1% TFA in CH_3CN. Approximately 3.0 ml fractions were collected manually and then analyzed on a Microbore HPLC (Applied Biosystems, model 120A) using a buffer system consisting of Buffer A: 0.06% TFA/dH2O and Buffer B: 0.05% TFA in 80% CH_3CN.20% dH_2O; a reversed-phase 2.1 × 150 mm column (Vydac C18) with a flow rate of 400 µl/min using a gradient of 5–95% B in 9 min. Fractions containing the purified peptides were pooled and freeze-dried.

Peptide characterization by analytical HPLC and Mass Spectrometry. The purity of the lyophilized peptides was verified by analytical reverse-phase HPLC on a Beckman Coulter System Gold, using an Agilent Zorbax-CN 4.6 x 50 mm (3.5 micron particle size) column at 500C. A 20–90% B gradient in 7 min at a flow rate of 1 ml/min was utilized. Buffer A was 0.1% TFA in dH_2O and Buffer B was 0.1% TFA in CH_3CN. Structures of the peptides were further confirmed by matrix-assisted laser desorption ionization time of flight mass spectrometry (MALDI-TOF-MS) on an Applied Biosystems Voyager DE instrument using alpha-cyano-4-hydroxycinnamic acid matrix. Representative profiles of HPLC and mass spectra MALDI/MS are shown for hPTH(1–34) (**Supplementary Fig. 8)** and for [K13TMR]hPTH(1-34) (**Supplementary Fig. 9)**.

Supplementary Results

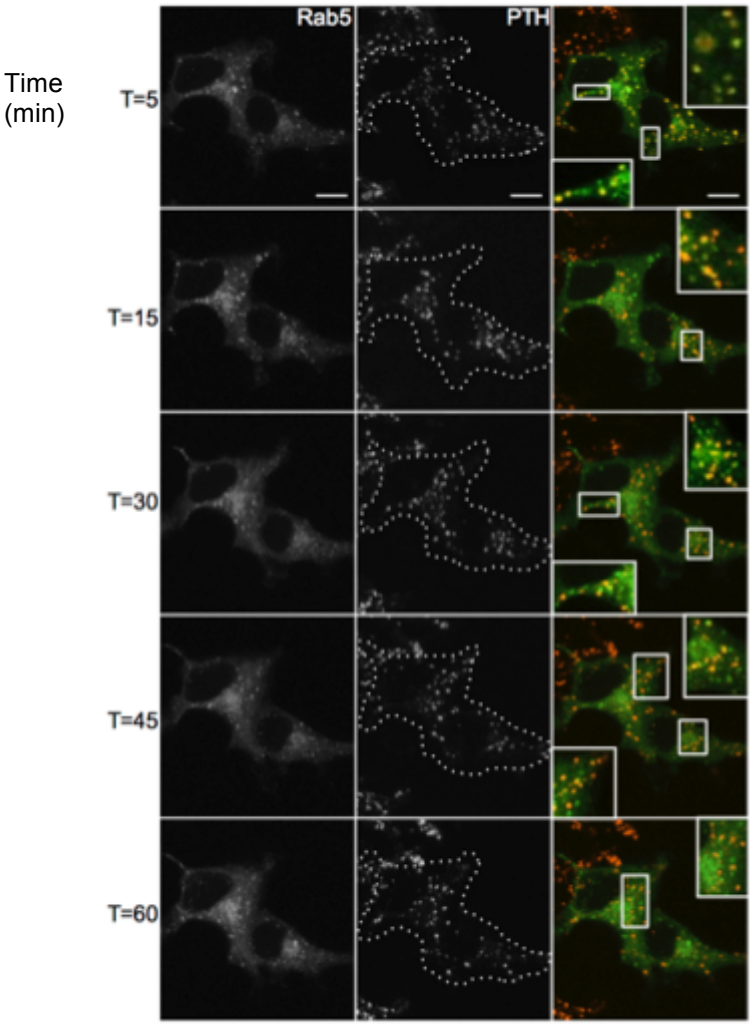

Supplementary Fig. 1. Co-localization of PTH^{TMR} (red) and Rab5^{GFP} (red). HEK-293 cells stably expressing the PTHR and Rab5^{GFP} were perfused with 100 nM PTH(1–34)^{TMR} for 30 s and then with buffer alone for the remainder of the experiment. The horizontal bar represents 10 μm. Microfilms are representative of n = 7 experiments used to calculate Pearson's correlation coefficient shown in Fig. 1b.

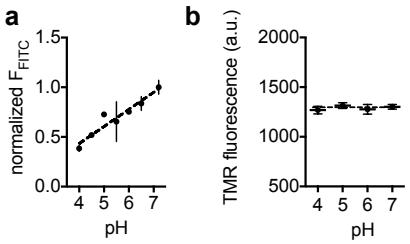

Supplementary Fig. 2. Recording pH using PTH^{FITC}. Standard plots showing the mean of PTH^{FITC} (**a**) or PTH^{TMR} (**b**) fluorescence against pH. Data represent mean values ± sem of $n = 5$ experiments.

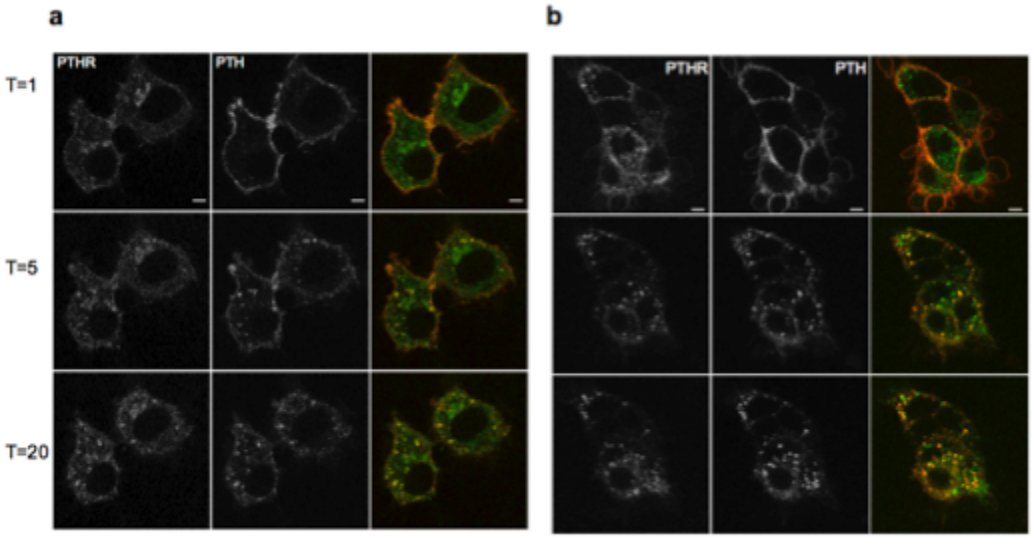

Supplementary Fig. 3. Trafficking of PTH^{TMR} and $PTHR^{GFP}$ were monitored in live HEK293 cells without (**a**) or with bafilomycin (**b**) by confocal scanning microscopy. Fluorescence micrographs showed individual channels for 100 nM $PTH(1{-}34)^{TMR}$ or $PTHR^{GFP}$. Time (T) in minutes. Scale bars, 10 μm.

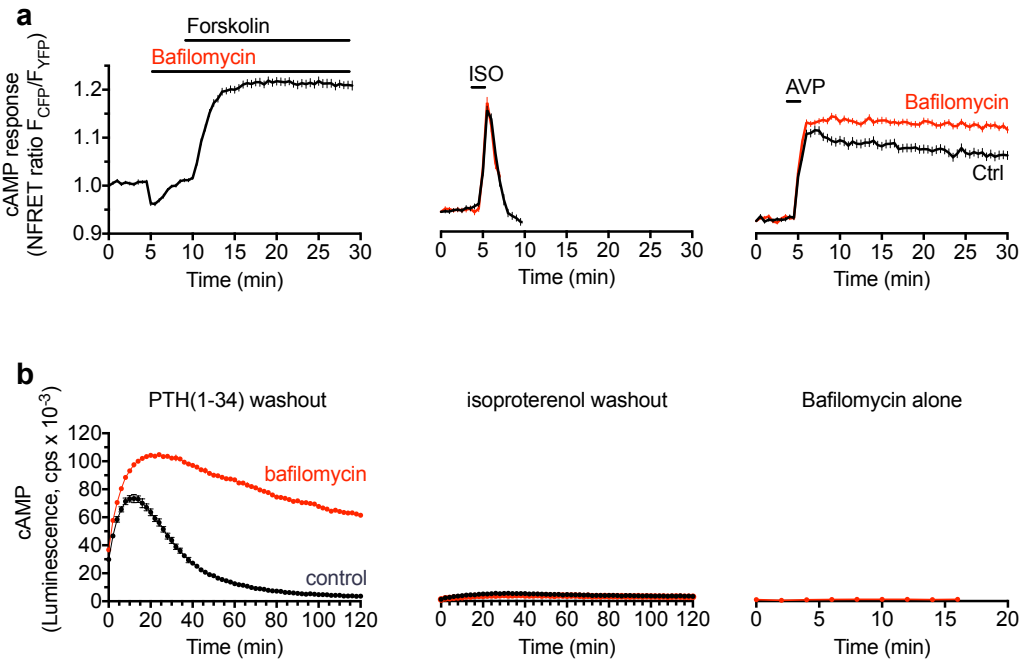

Supplementary Fig. 4. Effect of Bafilomycin-A1 on duration of signaling by PTH or other ligands. **(a)** FRET assay to record time-courses of cAMP production in response to forskolin (10 μM), isoproterenol (ISO, 10 μM), or vasopressin (AVP, 100 nM) alone (ctrl) or with bafilomycin (red) in single HEK293 cells stably expressing the PTHR, or the V2R. Data represent mean values ± s.e.m. of five independent experiments and $n > 50$ cells. **(b)** Bioluminiscence assay to monitor cAMP levels in HEK-293 cells stably expressing the PTHR and the luciferase-based cAMP reporter in 96-well plates. Cells were pre-loaded with luciferin for 30 min, then treated with buffer or Bafilomycin-A1 for 15 min, then with the indicated ligand for 15 min, then washed twice, and cAMP-dependent luminescence was recorded for 3 h in a PerkinElmer Plate reader. Data represent mean values ± s.e.m. of five independent experiments.

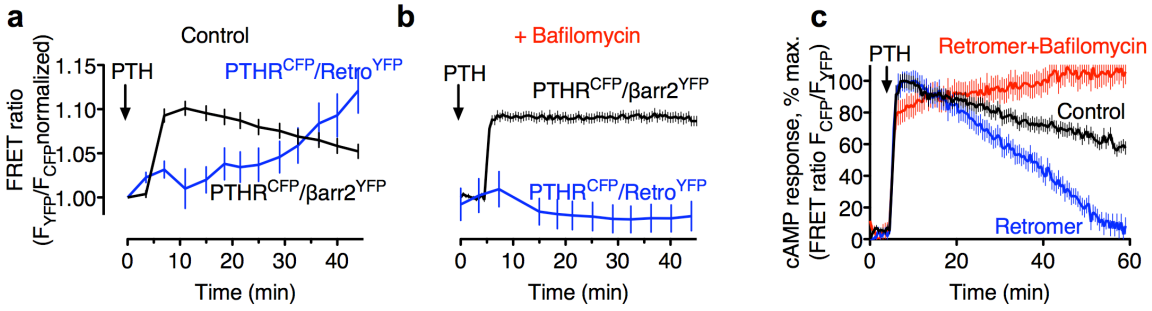

Supplementary Fig. 5. **Actions of β-arrestin 2 and retromer on PTHR regulated by the v-ATPase activity.** (**a–b**) Averaged time courses of interaction between PTHR and either β-arrestin2 or retromer subunit Vps29 recorded by changes of the normalized FRET ratio F_{YFP}/F_{CFP} in HEK-293 cells transiently expressing PTHR-CFP with either β-arrestin2-YFP or Vps29-YFP along with Vps26 and Vps35, and treated without (a) or with bafilomycin (b). Data represent mean values ± s.e.m. of three independent experiments and n = 46 (control) and n = 61 (bafilomycin) cells for PTHR–arrestin interactions; and n = 46 (control), and n = 32 (bafilomycin) cells for PTHR–Vps29 interactions. (**c**) Similar cAMP recording as in (a) and performed in HEK-293 cells stably expressing PTHR and transiently transfected to express Vps26, Vps29 and Vps35 (retromer). Data represent mean values ± s.e.m. of five independent experiments and n = 60 cells for each condition.

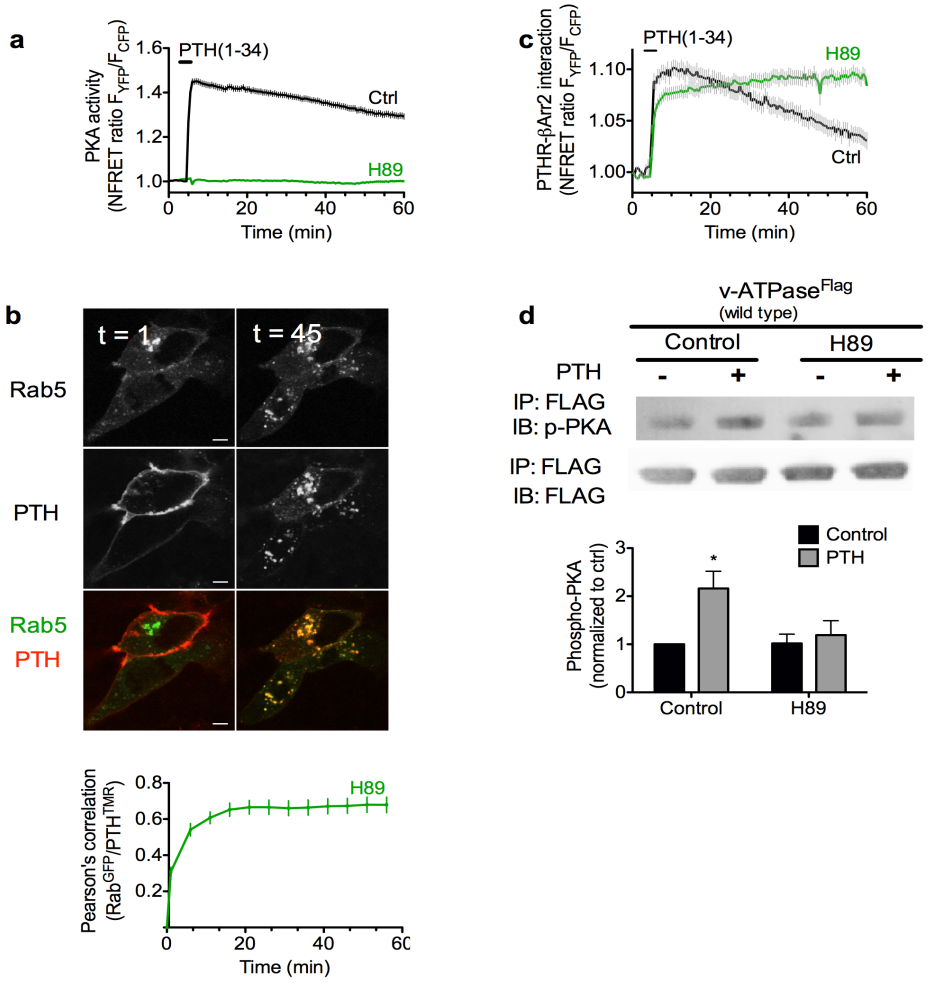

Supplementary Fig. 6. Effect of PKA on PTHR internalization and arrestin binding. (**a**) averaged time course of PKA activity measured by FRET in HEK293 cells stably expressing PTHR and a sensor for PKA activity (AKAR3) without (ctrl, black)) or with H89 (green). Cells were perfused with buffer or with 100 nM PTH (horizontal bar). Data represent mean values ± s.e.m. of four independent experiments and n = 114 (control) and n = 90 (H89) cells. (**b**) Pearson's analysis to quantify the change in PTHR localization with Rab5 when cells were treated with the PKA inhibitor H89 . Data were obtained from HEK-293 cells stably expressing PTHR and the early endosome marker, $Rab5^{GFP}$. Cells were briefly perfused (20 s) with 100 nM of $PTH(1\text{-}34)^{TMR}$ and then with buffer alone for the remainder of the experiment. Data represent the mean ± s.e.m. of three independent experiments and n = 24 cells. (**c**) Averaged time courses of interaction between PTHR and β-arrestin2 in HEK-293 cells treated without (ctrl) or with H89 (green), in response to 100 nM PTH. Data represent mean values ± s.e.m. of three independent experiments and n = 46 (control) and n = 30 (H89) cells. (**d**) Effect of H89 on PTH mediated phosphorylation of the v-ATPase using the PKA phosphorylation substrate-specific antibody (*upper*) and FLAG (*lower*). Bars represent mean values ± s.e.m of n = 5 ($^{*}P <$ 0.05).

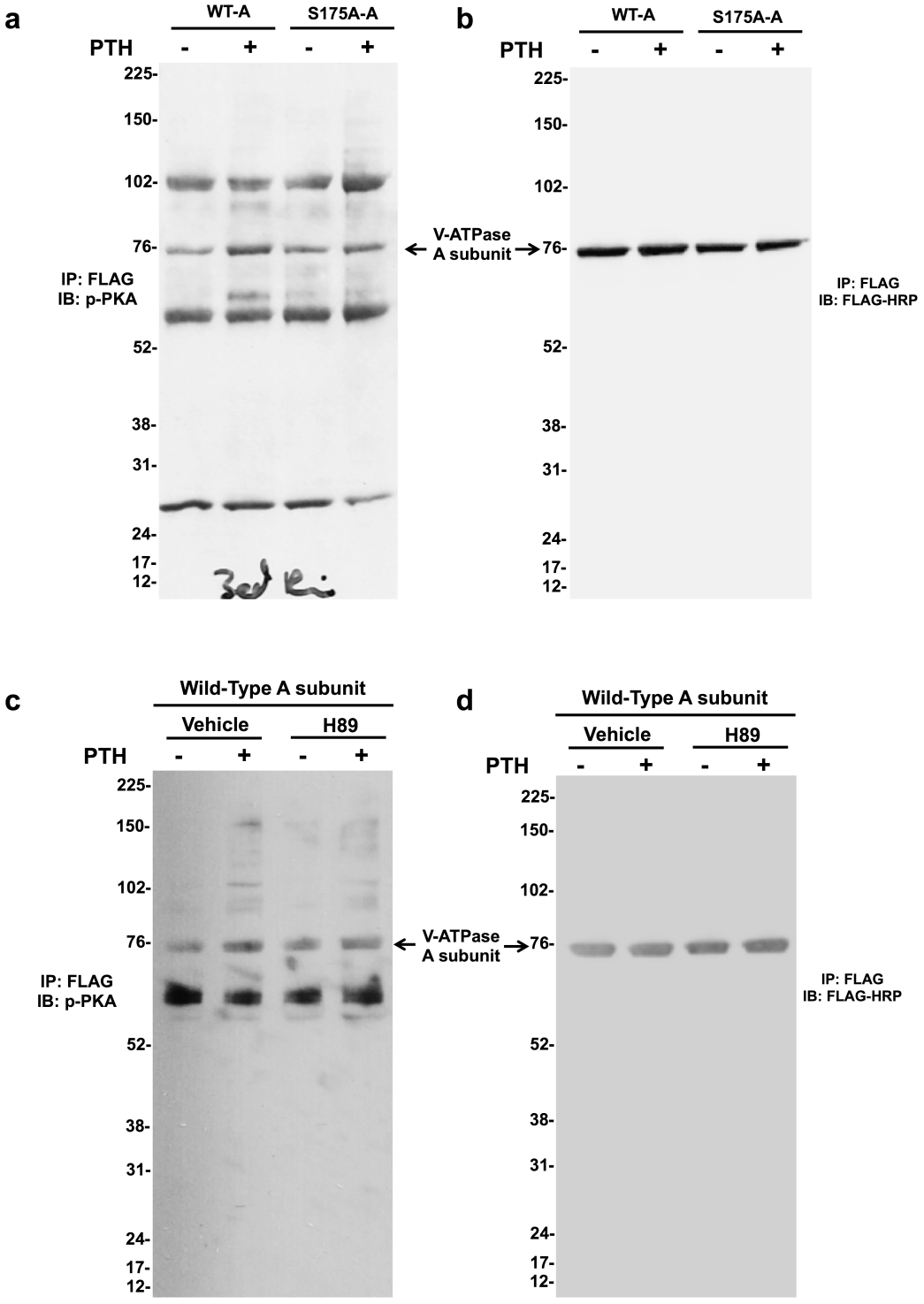

Supplementary Fig. 7. Full gel images. (a–d) full gel of experiments shown in Fig. 2a (a, b) and Suppl. Fig. 6d (c, d).

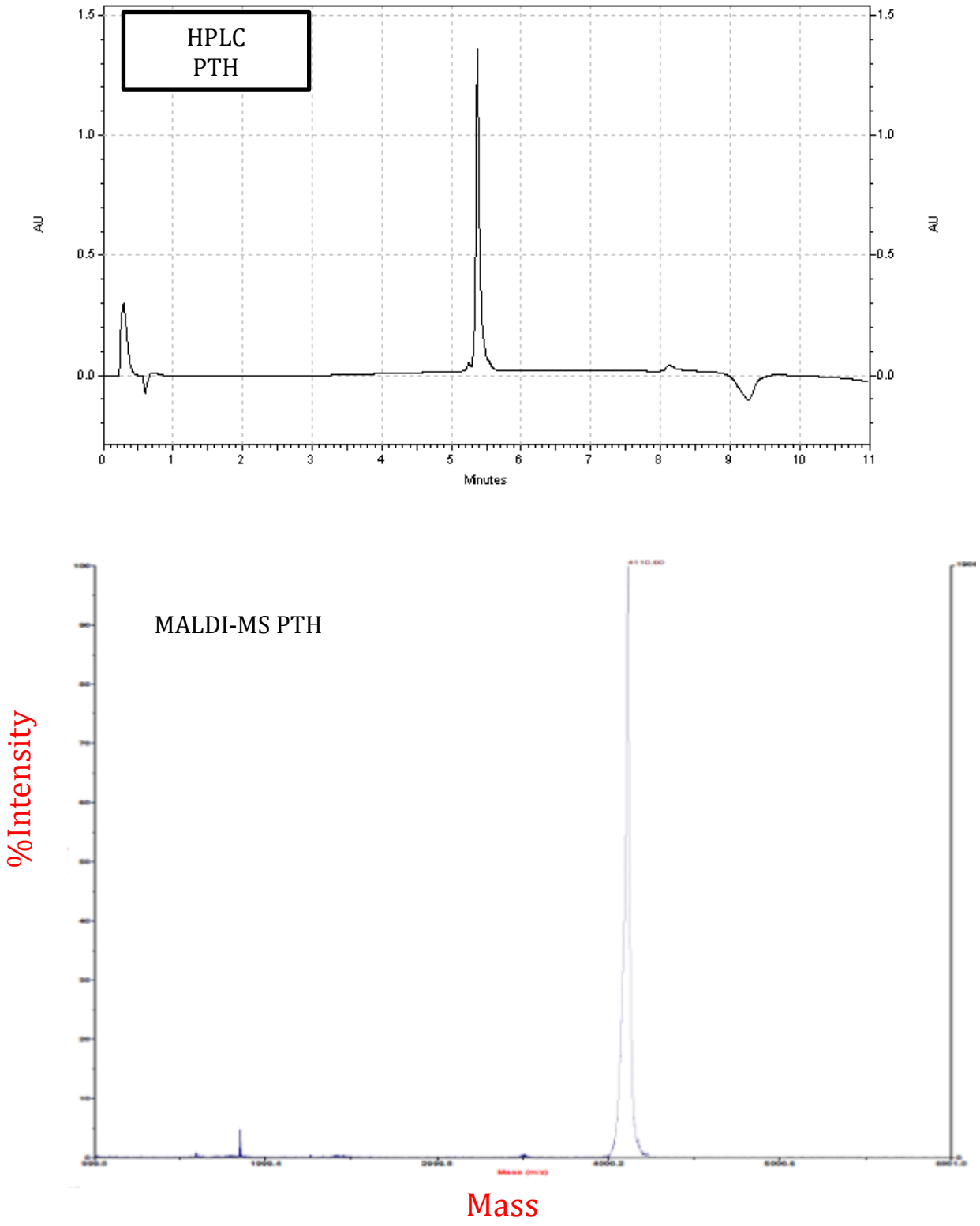

Supplementary Fig. 8. Analytical data of PTH(1-34) purification. Purification of human PTH(1–34) by high performance liquid chromatography (HPLC) (*upper panel*), and MALDI/MS fingerprint (*lower panel*).

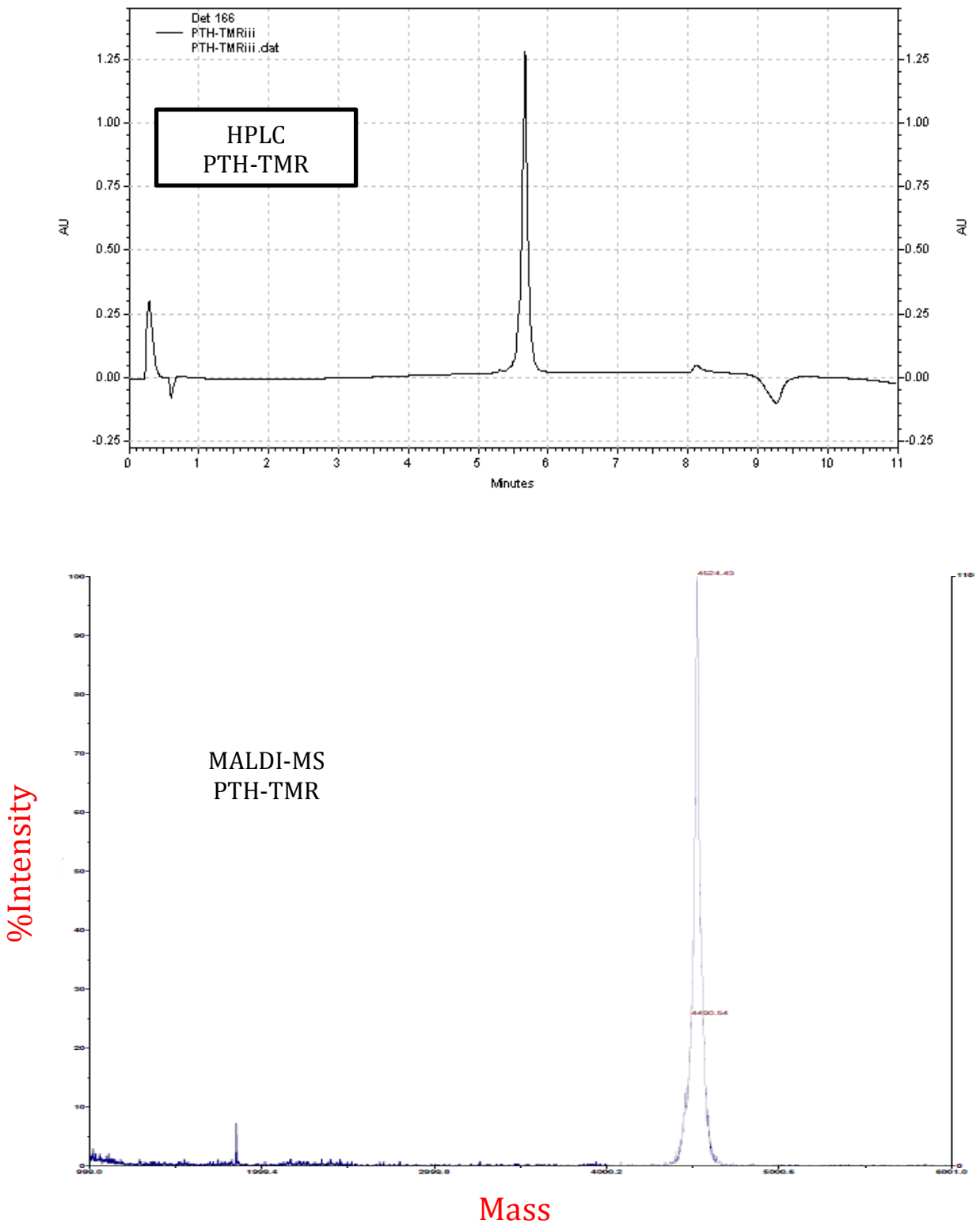

Supplementary Fig. 9. Analytical data of PTH(1–34)^{TMR} purification. Purification of human PTH(1–34) by high performance liquid chromatography (HPLC) (*upper panel*), and MALDI/MS fingerprint (*lower panel*).

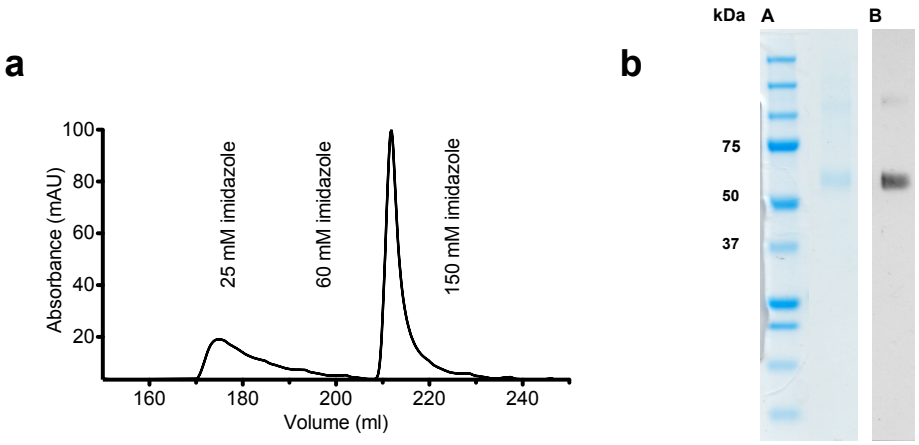

Supplementary Fig. 10. PTHR purification. (a). UV chromatogram of PTHR purification by using a His-select fast flow resin (Sigma) as previously described[9]. **(b)** 10 % SDS PAGE gel of PTHR purified to homogeneity in the presence of Fos-Choline-14, stained with Bradford (left), Western blot of purified receptor, probed with anti-His (right).